

School of Natural Sciences and Mathematics

***Relativistic Electron's Butterfly Pitch Angle Distribution
Modulated by Localized Background Magnetic Field
Perturbation Driven by Hot Ring Current Ions***

UT Dallas Author(s):

Lunjin Chen
Zhiyang Xia

Rights:

©2017 American Geophysical Union. All Rights Reserved.

Citation:

Xiong, Ying, Lunjin Chen, Lun Xie, Suiyan Fu, et al. 2017. "Relativistic electron's butterfly pitch angle distribution modulated by localized background magnetic field perturbation driven by hot ring current ions." *Geophysical Research Letters* 44(10), doi:10.1002/2017GL072558 4393-4400.

This document is being made freely available by the Eugene McDermott Library of the University of Texas at Dallas with permission of the copyright owner. All rights are reserved under United States copyright law unless specified otherwise.

RESEARCH LETTER

10.1002/2017GL072558

Key Points:

- Substorm ion injection produces magnetic dip in dayside radiation belt
- Magnetic dip produces energetic electron's butterfly PADs
- Electron inward transport contributes primarily to the electron's butterfly PADs

Correspondence to:

Y. Xiong,
yingxiongxyz@gmail.com

Citation:

Xiong, Y., L. Chen, L. Xie, S. Fu, Z. Xia, and Z. Pu (2017), Relativistic electron's butterfly pitch angle distribution modulated by localized background magnetic field perturbation driven by hot ring current ions, *Geophys. Res. Lett.*, 44, 4393–4400, doi:10.1002/2017GL072558.





Received 8 JAN 2017

Accepted 4 MAY 2017

Accepted article online 8 MAY 2017

Published online 21 MAY 2017

Relativistic electron's butterfly pitch angle distribution modulated by localized background magnetic field perturbation driven by hot ring current ions

Ying Xiong^{1,2,3} , Lunjin Chen³ , Lun Xie^{1,2}, Suiyan Fu^{1,2} , Zhiyang Xia³, and Zuyin Pu^{1,2} 
¹School of Earth and Space Sciences, Peking University, Beijing, China, ²PKU/UCLA Joint Research Institute in Science and Engineering, Peking University, Beijing, China, ³Physics Department, W. B. Hanson Center for Space Sciences, University of Texas at Dallas, Richardson, Texas, USA

Abstract Dayside modulated relativistic electron's butterfly pitch angle distributions (PADs) from ~200 keV to 2.6 MeV were observed by Van Allen Probe B at $L = 5.3$ on 15 November 2013. They were associated with localized magnetic dip driven by hot ring current ion (60–100 keV proton and 60–200 keV helium and oxygen) injections. We reproduce the electron's butterfly PADs at satellite's location using test particle simulation. The simulation results illustrate that a negative radial flux gradient contributes primarily to the formation of the modulated electron's butterfly PADs through inward transport due to the inductive electric field, while deceleration due to the inductive electric field and pitch angle change also makes in part contribution. We suggest that localized magnetic field perturbation, which is a frequent phenomenon in the magnetosphere during magnetic disturbances, is of great importance for creating electron's butterfly PADs in the Earth's radiation belts.

1. Introduction

The magnetic trapped energetic electrons encircling our planet form the Earth's electron radiation belts. The radiation belts generally consist of two distinct zones, the inner belt ($L = 1-2$) and the outer belt ($L = 3-8$), separated by a low flux "slot" region. The inner belt is relatively stable compared to the outer belt. The outer belt is very dynamic and dramatically changes during magnetic disturbances [e.g., Baker *et al.*, 2004; Horne *et al.*, 2005b; Chen *et al.*, 2007; Summers *et al.*, 2007; Reeves *et al.*, 2013; Thorne *et al.*, 2013; Xiong *et al.*, 2015]. Radiation belts electrons have three quasiperiodic motions: gyration around the ambient magnetic field, bounce along the background magnetic field, and drift around the Earth, each of which can be associated with an adiabatic invariant. Violation of these invariants can lead to the change of electron energy, pitch angle, and drift shell.

Electron's pitch angle is a key parameter to describe the motion and distribution of particles in phase space. The variation of the relativistic electron's pitch angle distributions is also of great importance in radiation belt physics. Different types of pitch angle distributions (PADs) can provide important information about the underlying physical processes that electron experienced, including wave-particle interaction and radial transport processes. On the other hand, different PADs can affect the loss and energization of the radiation belt electrons. High time and pitch angle resolution data from Van Allen Probes (VAP) provide us a great opportunity to investigate the relativistic electron's PADs in radiation belts.

The radiation belt electron's PADs can be classified into three categories: 90° peak (also known as pancake distribution), flat-top distribution, and butterfly distribution with a peak at off 90° [Gannon *et al.*, 2007; Gu *et al.*, 2011; Zhao *et al.*, 2014a, 2014b]. The pancake distribution is frequently observed in the radiation belts and can be produced by inward radial diffusion and wave-particle interaction with electron cyclotron harmonic waves [Lyons, 1974; Meredith *et al.*, 1999] and chorus waves [Ni *et al.*, 2015]. The flat-top distribution can be treated as the transition between pancake and butterfly PAD. As for the butterfly distribution, the generation mechanisms are relatively complicated and incomplete.

The butterfly PAD can be observed during geomagnetic quiet times and disturbances. During the quiet time, electron's butterfly PAD usually takes place at nightside with $L = 5-9$ [Roederer, 1967; West *et al.*, 1973; Selesnick and Blake, 2002]. It is produced by the drift shell splitting effect due to the day-night asymmetry

of the Earth magnetic field. The 90° electrons can drift further than electrons of smaller pitch angles and will be lost when their drift orbits come across the magnetopause. This mechanism is called as magnetopause shadowing effect [West *et al.*, 1973]. During magnetic activities, the observation of butterfly PAD can be located within $L = 6$ at all magnetic local time (MLT) [Lyons and Williams, 1975; Sibeck *et al.*, 1987]. Currently, seven mechanisms have been proposed to explain the formation of the butterfly PAD during magnetic activities: (a) wave-particle interaction with magnetosonic waves and chorus waves [Horne *et al.*, 2005a; Xiao *et al.*, 2015; Li *et al.*, 2016b, 2016a; Chen *et al.*, 2015; Maldonado *et al.*, 2016], (b) nonlinear resonance with oblique electromagnetic ion cyclotron waves [Wang *et al.*, 2016], (c) wave-particle interaction with hiss waves, lightning-generated whistlers and ground VLF transmitters [Albert *et al.*, 2016], (d) outward adiabatic transports [Su *et al.*, 2010], (e) magnetopause shadowing effect [e.g., Wilken *et al.*, 1986], (f) substorm injection combined with drift shell splitting [Sibeck *et al.*, 1987], and (g) nonadiabatic scattering due to the field line curvature scattering [Artemyev *et al.*, 2015] and adiabatic effect caused by ring current through the conservation of electron's magnetic moment [Lyons, 1977].

In this paper, we report for the first time an event of butterfly PADs of relativistic electrons modulated by the background magnetic compressional component from Van Allen Probes observation. Such localized modulation of the electron's butterfly PAD is unlikely to be explained by the mechanisms mentioned above. It leads us to promote a new mechanism suitable for this observation. The modulation of butterfly PAD is reported in section 2. Section 3 is the test particle simulation of the modulated butterfly PAD, where we propose a new mechanism for the formation of the butterfly PAD. In section 4, we discuss and summarize our results.

2. Observations

A modulated electron's butterfly PAD event was measured by VAP B during a moderate magnetic storm ($Dst = -40$ nT) on 15 November 2013. The VAP B travels near the magnetic equatorial plane (inclination 10.2°) with highly elliptical orbit (perigee $\sim 1.1 R_E$, apogee $\sim 5.9 R_E$) [Mauk *et al.*, 2013]. It is ideally suited to measure the equatorial electron PADs. In this study, the particle data are measured by Magnetic Electron Ion Spectrometer (MagEIS) [Blake *et al.*, 2013], Relativistic Electron-Proton Telescope (REPT) [Baker *et al.*, 2012], and Radiation Belt Storm Probes Ion Composition Experiment (RBSPICE) [Mitchell *et al.*, 2013]. The wave and ambient magnetic field data are measured by the Electric and Magnetic Field Instrument Suite and Integrated Science (EMFISIS) [Kletzing *et al.*, 2013].

On 15 November 2013, there is a moderate magnetic storm with $Dst = -40$ nT. Modulatory relativistic electron's butterfly PADs take place during the main phase of the storm, which is recorded by the VAP B satellite near $L = 5.3$ over the time period marked by the two vertical dashed lines in Figure 1. Figures 1g–1k show electron PAD measurement by MagEIS and REPT onboard over the energy range from hundreds of keV to MeV. Solar wind speed and dynamic pressure remain nearly constant during the observation of modulated relativistic electron's butterfly PADs (Figures 1c and 1d, between the two vertical red dashed lines). Hiss waves are observed during the event, but there is not any modulated signature with a period of 20 min. The magnetosonic waves are very weak and are not present in the corresponding modulatory signatures. Figure 1n plots the background magnetic field perturbation in the SM coordinate. The mean magnetic field is obtained by linearly fitting the observed B field during two time intervals (21:30–22:00 and 22:57–23:00) when the pressures change slowly. It is clearly seen that Z component (nearly field aligned) of magnetic perturbation in the SM coordinate system is dominant over the other two components. These butterfly PADs are modulated (period ~ 20 min) by the background magnetic field dips (especially the B_z component). These B_z perturbations are associated with enhanced anisotropic ion fluxes over 60–100 keV (Figures 1l–1m), which is likely due to the impulsive injections of hot ring current ions during the substorm activities (Figure 1e).

Figures 2a and 2b show the perpendicular thermal pressure perturbation of hot ring current ions and magnetic pressure perturbation, respectively. Since proton, helium, and oxygen ions show injection features, they are the major components of the ring current. The total perpendicular thermal pressure is obtained by summing the perpendicular thermal pressure of protons over the four energy channels (62.74 keV, 73.57 keV, 84.40 keV, and 97.94 keV), helium over the five energy channels (65 keV, 84 keV, 110 keV, 142 keV, and 184 keV), and oxygen over the four energy channels (64 keV, 106 keV, 142 keV, and 184 keV):

$$P_{\text{thermal}} = \frac{1}{2} \sum m \int_0^{2\pi} d\phi \int v_{\perp}^2 \cdot f(v, \theta) \cdot v^2 \cdot \sin \theta \cdot d\theta \cdot dv \quad (1)$$

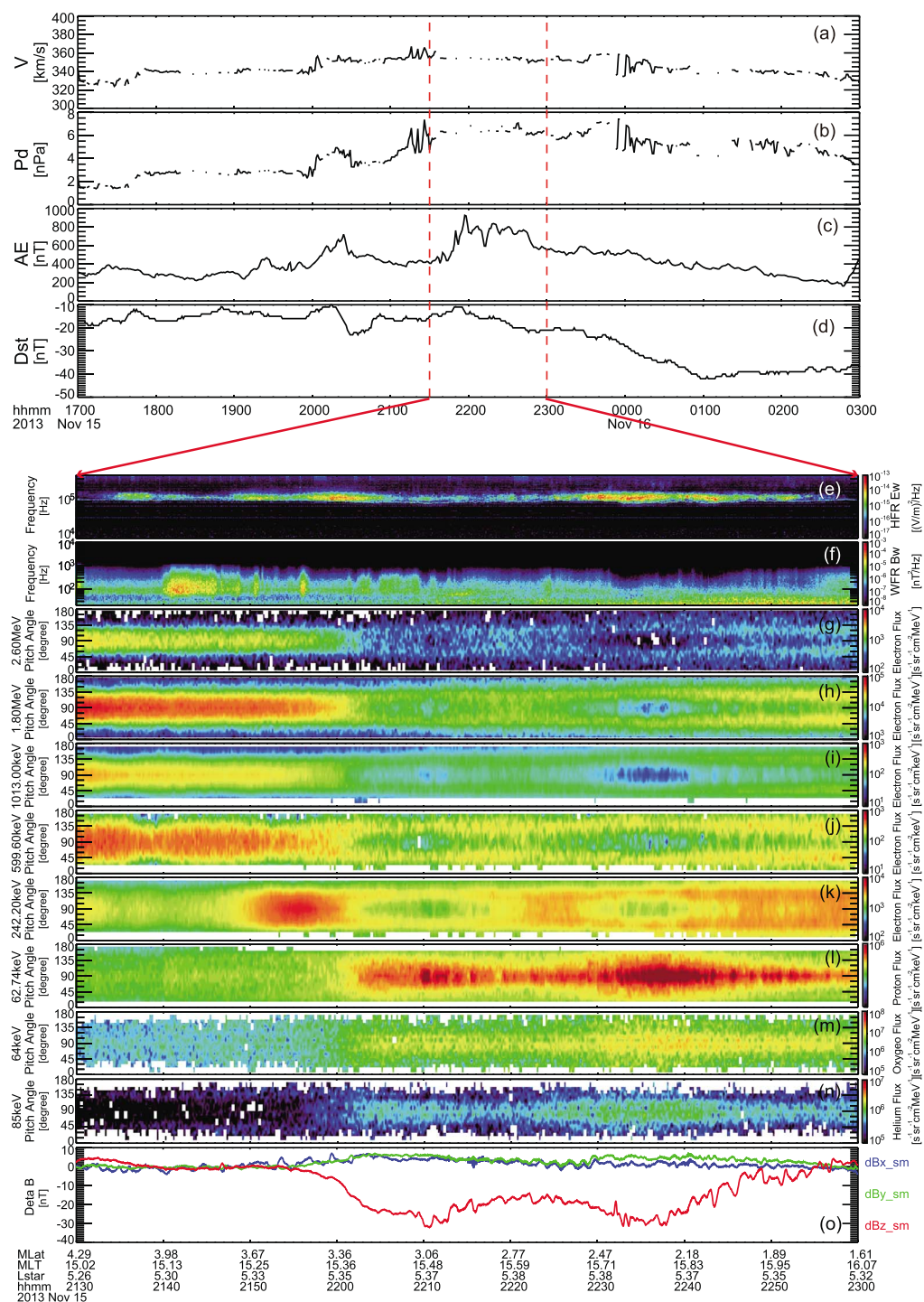


Figure 1. Observation of modulated electron's butterfly PADs. (a, b) Solar wind parameters and (c, d) geomagnetic indices, (e, f) the wave measurements, (g–k) modulated butterfly PADs from 200 keV to 2.6 MeV electron, (l, m) hot ring current ion injection, (n) background magnetic field perturbation in the solar magnetic coordinate system, and (o) measured B field subtract 90 min running average B field.

where m is the rest mass of the ions, θ is the pitch angle, v is the speed, and $f(v, \theta)$ is the phase space density which can be obtained from the number flux $j(v, \theta)$ through $f(v, \theta) = \frac{m^3 j(v, \theta)}{p^2}$, where p is the momentum. The magnetic pressure is calculated through $P_{\text{mag}} = \frac{B^2}{2\mu_0}$, where B is the background magnetic field and μ_0 is the vacuum permeability.

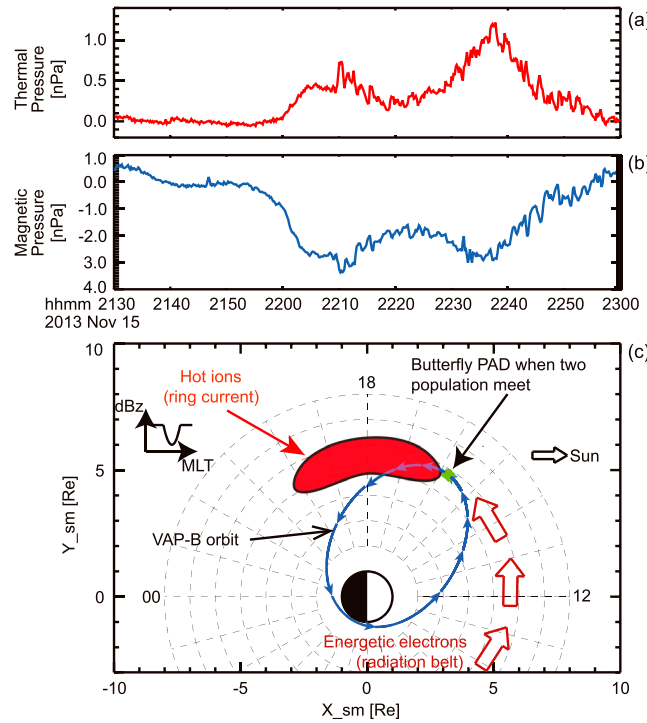


Figure 2. The physical scenario of producing relativistic electron's butterfly pitch angle distribution. (a) Perpendicular thermal pressure perturbation, (b) magnetic pressure perturbation, and (c) diagram of dynamic process between hot ring current ions and energetic electrons.

distribution to a magnetic field dip according to observed parameters and compare our results to the observed response. We use test particle simulation to investigate the changes of pitch angle, L shell, and energy for different pitch angle electrons at different energies when they travel through the B_z dip structure. Based on Liouville's theorem, the observed PADs can be reconstructed if the initial steady state flux model is provided.

3.1. Magnetic Field Model

As Figure 2c shows, the B_z dip structure is associated with ring current ions, which carry a localized thermal pressure and experience drift from duskside to dayside. When the ring current ions met with the eastward drift radiation belt electrons at the VAP B position marked as the green line in Figure 2c (from 22:00 to 22:20), the electron butterfly PADs were observed.

For test particle simulation, the magnetic field model is constructed by adding a modeled B_z perturbation to a background dipole field:

$$\mathbf{B}(L, MLT, MLat, t) = \mathbf{B}_{\text{dipole}}(L, MLT, MLat, t) + dB_z(L, MLT, MLat, t) \cdot \mathbf{e}_z \quad (2)$$

We adopt a localized dB_z structure that moves azimuthally with hot ions. We estimate the azimuthal speed, $0.055^\circ/\text{s}$, based on the magnetic gradient and curvature drift in the dipole field for hot ion drift with energy 80 keV and pitch angle 90° . Since the speed of VAP B ($0.003^\circ/\text{s}$) was much smaller than the azimuthal speed of the dB_z structure, we assumed that the observations during the modulation period (20 min) occurred in the same location. Then, the azimuthal range of the dB_z structure can be estimated by $0.055^\circ/\text{s} \times 20 \text{ min}$, corresponding to 4.4 h in MLT. The dB_z magnetic field consists of three parts, L distribution (scale = 0.8), MLT distribution (scale = 4.4 h), and magnetic latitude (MLat) distribution (scale = $[-15, 15]$)

$$dB_z(L, MLT, MLat, t) = dB_{z0} \cdot f_L(L) \cdot f_{MLT}(MLT, t) \cdot f_{MLat}(MLat) \quad (3)$$

The baselines of the thermal and magnetic pressure are obtained by linearly fitting the data during the same two time periods mentioned above (21:30 to 22:00 and 22:57 to 23:00) when the pressures change slowly. Pressure perturbation is obtained by the difference between the original and the baseline pressures. The red and blue traces in Figures 2a and 2b are the thermal and magnetic pressure perturbations, respectively. The negative correlation between this two pressures and comparable fluctuation amplitudes supports that the hot ring current ion injection produces the ambient magnetic field perturbation. The thermal pressure perturbation of proton is slightly greater than the pressure perturbation of oxygen.

3. Test Particle Simulation

In order to sort out the physical mechanism responsible for the modulation of the electron butterfly PADs through hundreds of keV to MeV by the compressional magnetic field component perturbation, we simulate the response of electron pitch angle

Table 1. Fitting Coefficients of the Initial Flux Model^a

Energy	<i>a</i>	<i>b</i>	<i>c</i>
599.6 keV	−1.28(RMSE = 0.21)	−1.28(RMSE = 0.06)	0.53(RMSE = 0.04)
1013 keV	−1.28(RMSE = 0.21)	−1.35(RMSE = 0.09)	0.86(RMSE = 0.15)
1.8 MeV	−1.75(RMSE = 0.01)	−1.01(RMSE = 0.03)	1.08(RMSE = 0.15)
2.6 MeV	−1.75(RMSE = 0.01)	−1.24(RMSE = 0.06)	1.06(RMSE = 0.31)

^aRMSE is the root-mean-square error which indicates goodness of fitting.

where dB_{z0} is -30 nT, which is about the amplitude of the dB_z structure shown as Figure 1n, the radial profile of the dB_z structure is in Gaussian shape

$$f_L(L) = e^{\frac{-(L-L_0)^2}{2\delta L^2}} \quad (4)$$

where L_0 is 5.33 and δL is 0.2. The MLat profile is also in Gaussian shape:

$$f_{\text{MLat}}(\text{MLat}) = e^{\frac{\text{MLat}^2}{2\delta \text{MLat}^2}} \quad (5)$$

where δ MLat is 4° (~ 0.07 rad). The MLT profile is a little complicated like current sheet profile:

$$f_{\text{MLT}}(\text{MLT}) = \frac{\tanh(\text{MLT}-\text{MLT}_c(t) + \delta \text{MLT}) + \tanh(-\text{MLT} + \text{MLT}_c(t) + \delta \text{MLT})}{2 \tanh(\delta \text{MLT})} \quad (6)$$

where $\text{MLT}_c(t)$ is the center of B_z perturbation, δMLT is 1.1 h. Thus, time-varying magnetic field can be described as a dipole field superposed a dB_z structure centered at the equatorial plane with $L = 5.36$, drifting westward at an angular speed of $0.055^\circ/\text{s}$.

3.2. Initial Flux Model

We construct the data-based initial steady state flux model for four different energy channels separately, in the following form:

$$j(E_k, L, \alpha) = j_0 \cdot 10^{[a(E_k - E_{k0})]} \cdot \sin^c(\alpha) \quad (7)$$

where E_k is a dimensionless quantity normalized by 1 MeV and j_0 is the averaged 90° flux before the modulation (21:59 to 22:00), E_{k0} is the energy channel normalized by 1 MeV, L_0 is 5.33, α is the equatorial pitch angle, and a , b , c are the coefficients to be fit and describe the distribution in energy, L shell, and pitch angle, respectively. The initial pitch angle distributions are obtained by fitting the data 1 min before the modulation (21:59 to 22:00) where $L = 5.35$. The energy spectra are calculated for two different instruments, REPT and MagEIS, respectively. The data used to fit the power law form of the energy spectra are also 1 min before the modulation. We obtain the radial profiles by fitting the data 1 h before the modulation (21:00 to 22:00) with L range from 5.12 to 5.35. Table 1 shows the fitting coefficients and root-mean-square of errors for coefficient a , b , and c for four different energy channels. The electron fluxes decrease as energy and/or L shell increases. The coefficient c is positive and increases as energy, indicating that the pitch angle distributions are more 90° peaked for high energies.

3.3. Simulation Results

Test particle simulation using guiding center equations [Elkington *et al.*, 2002] without considering the direct electric field is used to simulate the electron PAD response at the fixed observation location to a moving dB_z structure. Electrons at the observation location at a given t with a given α and E_k are tracked backward to initial time ($t = 0$) with corresponding E_{k0} , α_0 , and L_0 , where is outside of the B_z perturbation. Based on Liouville's theorem, we can derive the observed the electron flux $j_{\text{ob}}(E_k, L, \alpha) = \frac{p_{\text{ob}}^2 j_0(E_{k0}, L_0, \alpha_0)}{p_0^2}$. When the relative changes in energy, L shell, and equatorial pitch angle are small, one can obtain the following relation through Taylor expansion:

$$j_{\text{ob}}(E_k, L, \alpha) = \frac{p_{\text{ob}}^2}{p_0^2} j_0(E_k, L, \alpha) \cdot (1 + a \cdot dE_k + b \cdot dL + c \cdot \cot \alpha d\alpha) \quad (8)$$

where the changes of energy, L shell, and pitch angle (dE_k , dL , $d\alpha$) are obtained by simulating the electron motion under the time-varying magnetic field using guiding center equations. The observed electron momentum and original electron momentum are denoted as p_{ob} and p_0 , respectively.

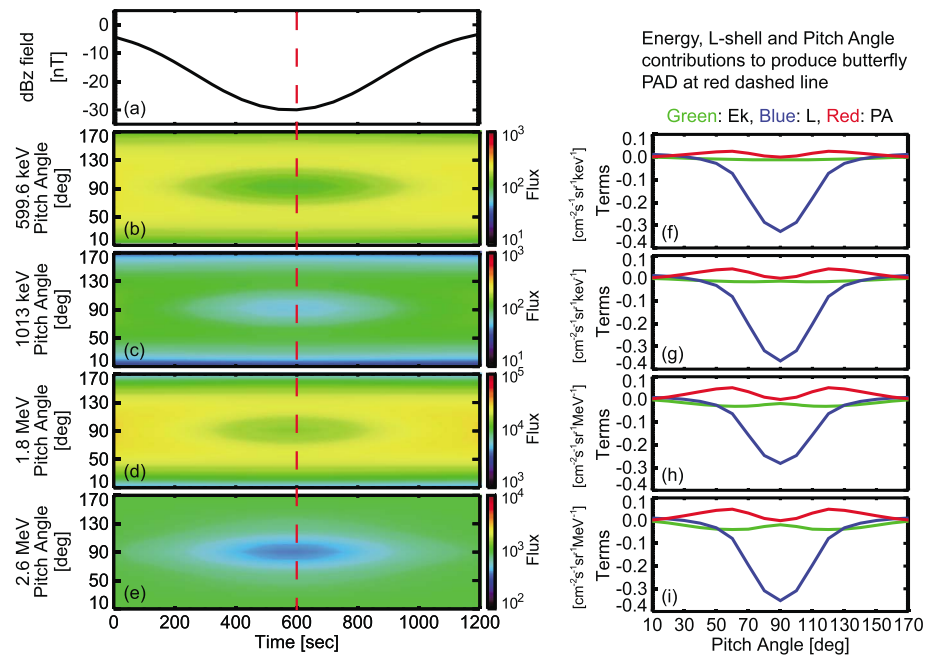


Figure 3. Test particle simulation results. (a) B_z perturbation. (b–e) Reproduced electron's butterfly pitch angle distributions for 599.6 keV, 1013 keV, 1.8 MeV, and 2.6 MeV, respectively. The red dashed line denotes the center of the B_z perturbation. (f–i) The contributions of the change of electron energy (green line), L shell (blue line), and equatorial pitch angle (red line) to the formation of electron butterfly pitch angle distributions for each four energy electrons at the center of the B_z dip.

According to the backward tracing results, the changes of momentum for all pitch angles are about 1–2%, the ratio of the observed momentum and initial momentum can be treated as 1. Thus, the simulated pitch angle distribution changes are controlled by three dimensionless terms: $a \cdot dE_k$, $b \cdot dL$, and $c \cdot \cot \alpha d\alpha$, which are related to the changes of energy, L shell, and pitch angle. Figures 3a–3e show the simulation results of PAD at different energies as the moving dB_z dip passes through the observation location. The vertical red line marked the time t_{\min} when B_z minimum passes the observation location. Butterfly PADs observed at four energy channels are reproduced during the B_z dip (see Figures 3a–3e). Figures 3f–3i illustrate the changes of energy ($a \cdot dE_k$), L shell ($b \cdot dL$), and pitch angle ($c \cdot \cot \alpha d\alpha$) as a function of observed pitch angle at t_{\min} .

The backward tracing results show that (a) off 90° electrons lose more energy than 90° electrons through Fermi deceleration due to the conservation of the second adiabatic invariant, and the contribution of the energy change to creating relativistic electron's butterfly PADs became greater as energy increases. (b) Larger pitch angle electrons are transported from higher L shell, and the inward transport contributes primarily to producing relativistic electron's butterfly PADs. (c) The decrease of pitch angle is greater for off 90° electrons than 90° electrons, which contributes positively to the formation of the relativistic electron's butterfly PADs especially at higher energy. As shown in Figure 3, the electron deceleration ($a \cdot dE_k$ is less than 5% contribution) and pitch angle decrease ($c \cdot \cot \alpha d\alpha$ is larger than $a \cdot dE_k$ but also less than 10% contribution) in part contribute to the formation of the electron butterfly PADs. Since coefficient b is negative indicating a negative flux gradient in L for our event, the electron inward transport ($b \cdot dL$ is more than 30% contribution) contributes primarily to creating electron butterfly PADs. For the case of a positive flux gradient, it can contribute to producing the electron 90° peak PADs.

4. Conclusions and Discussion

In this paper, we investigated the formation mechanism of the dayside modulated relativistic electron's butterfly PADs at $L = 5.3$ using a test particle simulation, where we do not consider the contribution of the eastward inductive electric field (due to the local magnetic field perturbation) to the electric drift velocity. We estimate the inductive electric field based on our time-varying magnetic field model and find that the outward drift speed arising from the inductive electric field is much smaller than the inward drift speed due to

the azimuthal gradient of magnetic field. In addition, we check the electric field data from the Electric Fields and Waves (EFW) [Wygant *et al.*, 2013]. Although the electric field measurements are only available within the satellite's spin plane, we use them to do a rough estimate of the outward drift speed associated with azimuthal electric field and find that it is still only about 20% of the drift speed caused by the magnetic field gradient. The model of such electric field may be complicated, but, fortunately, our analysis above does show that the electron's radial drift is dominated by gradient of magnetic field, and thus, the main physics of relativistic electron transport is captured by our current model. With the initial equilibrium flux model, we evaluate the contributions of the changes of energy, L shell, and equatorial pitch angle and reconstruct the observed relativistic electron's PADs and demonstrated that localized ambient magnetic field dip could produce the modulatory of electron butterfly PADs. Our principal conclusions are summarized as follows:

1. The dayside relativistic electron's butterfly PADs (~ 200 keV to 2.6 MeV) are reported for the first time and are modulated by localized magnetic dips.
2. The magnetic dips are driven by hot ring current ion (60–100 keV proton and 60–200 keV helium and oxygen ion) injections during substorm activities.
3. A negative radial flux gradient contributes primarily to the formation of modulated electron butterfly PADs through inward transport due to azimuthal electric field induced by the moving localized B_z perturbation.
4. Deceleration due to inductive electric field and pitch angle change also make in part contribution to producing electron butterfly PADs.

Substorms are the most common geomagnetic disturbance in the Earth's magnetosphere and usually accompany magnetic storms [e.g., Daglis *et al.*, 1999]. Impulsive substorm injection of tens to few hundred keV ions from the magnetic tail to the inner magnetosphere is one of the significant sources of the ring current ions [e.g., Reeves, 2003]. The impulsive injections of ring current ions can produce the localized magnetic dips as shown in section 2 due to the presence of the enhanced thermal pressure carried by these ring current ions. Therefore, we suggest that localized magnetic field perturbation, which is a frequent phenomenon in the magnetosphere, is of great importance for creating electron's butterfly PADs in the Earth's radiation belts. We have already found 76 modulated relativistic electron's butterfly PADs cases accompanied by the localized magnetic dips during the era of the Van Allen Probes, and the statistical characteristics will be discussed in the future work.

Acknowledgments

This work was supported by NSFC grants 41274167, 41674164, 41474139, and 41421003; NSF grants 1103064 through the Geospace Environment Modeling program; and the AFOSR grant of FA9550-16-1-0344. We acknowledge the Van Allen Probe ECT, RBSPICE, EMFISIS, and EFW teams for data usage. The ECT, RBSPICE, EMFISIS, and EFW data used in the study are obtained from <http://www.rbsp-ect.lanl.gov>, <http://rbspice.ftccs.com>, <http://emfisis.physics.uiowa.edu/>, and <http://www.space.umn.edu/rbspew-data/>, respectively. The solar wind parameters and geomagnetic indices are obtained from the SFC/SPDF OMNIWeb interface at <http://omniweb.gsfc.nasa.gov>.

References

- Albert, J. M., M. J. Starks, R. B. Horne, N. P. Meredith, and S. A. Glauert (2016), Quasi-linear simulations of inner radiation belt electron pitch angle and energy distributions, *Geophys. Res. Lett.*, **43**, 2381–2388, doi:10.1002/2016GL067938.
- Artemyev, A. V., O. V. Agapitov, F. S. Mozer, and H. Spence (2015), Butterfly pitch angle distribution of relativistic electrons in the outer radiation belt: Evidence of nonadiabatic scattering, *J. Geophys. Res. Space Physics*, **120**, 4279–4297, doi:10.1002/2014JA020865.
- Baker, D. N., S. G. Kanekal, X. Li, S. P. Monk, J. Goldstein, and J. L. Burch (2004), An extreme distortion of the Van Allen belt arising from the 'Halloween' solar storm in 2003, *Nature*, **432**(7019), 878–881, doi:10.1038/nature03116.
- Baker, D. N., et al. (2012), The Relativistic Electron-Proton Telescope (REPT) instrument on board the Radiation Belt Storm Probes (RBSP) spacecraft: Characterization of Earth's radiation belt high-energy particle populations, *Space Sci. Rev.*, **179**(1–4), 337–381, doi:10.1007/s11214-012-9950-9.
- Blake, J. B., et al. (2013), The Magnetic Electron Ion Spectrometer (MAGIS) instruments aboard the Radiation Belt Storm Probes (RBSP) spacecraft, *Space Sci. Rev.*, **179**(1–4), 383–421, doi:10.1007/s11214-013-9991-8.
- Chen, L., A. Maldonado, J. Bortnik, R. M. Thorne, J. Li, L. Dai, and X. Zhan (2015), Nonlinear bounce resonances between magnetosonic waves and equatorially mirroring electrons, *J. Geophys. Res. Space Physics*, **120**, 6514–6527, doi:10.1002/2015JA021174.
- Chen, Y., G. D. Reeves, and R. H. W. Friedel (2007), The energization of relativistic electrons in the outer Van Allen radiation belt, *Nat. Phys.*, **3**(9), 614–617, doi:10.1038/nphys655.
- Daglis, I. A., R. M. Thorne, W. Baumjohann, and S. Orsini (1999), The terrestrial ring current: Origin, formation, and decay, *Rev. Geophys.*, **37**(4), 407–438, doi:10.1029/1999RG900009.
- Elkington, S. R., M. K. Hudson, M. J. Wiltberger, and J. G. Lyon (2002), MHD/particle simulations of radiation belt dynamics, *J. Atmos. Sol. Terr. Phys.*, **64**(5–6), 607–615, doi:10.1016/S1364-6826(02)00018-4.
- Gannon, J. L., X. Li, and D. Heynderickx (2007), Pitch angle distribution analysis of radiation belt electrons based on Combined Release and Radiation Effects Satellite Medium Electrons A data, *J. Geophys. Res.*, **112**, A05212, doi:10.1029/2005JA011565.
- Gu, X., Z. Zhao, B. Ni, Y. Shprits, and C. Zhou (2011), Statistical analysis of pitch angle distribution of radiation belt energetic electrons near the geostationary orbit: CRRES observations, *J. Geophys. Res.*, **116**, A01208, doi:10.1029/2010JA016052.
- Horne, R. B., et al. (2005a), Wave acceleration of electrons in the Van Allen radiation belts, *Nature*, **437**(7056), 227–230, doi:10.1038/nature03939.
- Horne, R. B., R. M. Thorne, S. A. Glauert, J. M. Albert, N. P. Meredith, and R. R. Anderson (2005b), Timescale for radiation belt electron acceleration by whistler mode chorus waves, *J. Geophys. Res.*, **110**, A03225, doi:10.1029/2004JA010811.
- Kletzing, C. A., et al. (2013), The Electric and Magnetic Field Instrument Suite and Integrated Science (EMFISIS) on RBSP, *Space Sci. Rev.*, **179**(1–4), 127–181, doi:10.1007/s11214-013-9993-6.
- Li, J., et al. (2016a), Formation of energetic electron butterfly distributions by magnetosonic waves via Landau resonance, *Geophys. Res. Lett.*, **43**, 3009–3016, doi:10.1002/2016GL067853.

- Li, J., et al. (2016b), Ultrarelativistic electron butterfly distributions created by parallel acceleration due to magnetosonic waves, *J. Geophys. Res. Space Physics*, *121*, 3212–3222, doi:10.1002/2016JA022370.
- Lyons, L. R. (1974), Electron diffusion driven by magnetospheric electrostatic waves, *J. Geophys. Res.*, *79*(4), 575–580, doi:10.1029/JA079i004p00575.
- Lyons, L. R. (1977), Adiabatic evolution of trapped particle pitch angle distributions during a storm main phase, *J. Geophys. Res.*, *82*(16), 2428–2432, doi:10.1029/JA082i016p02428.
- Lyons, L. R., and D. J. Williams (1975), The quiet time structure of energetic (35–560 keV) radiation belt electrons, *J. Geophys. Res.*, *80*(7), 943–950, doi:10.1029/JA080i007p00943.
- Maldonado, A. A., L. Chen, S. G. Claudepierre, J. Bortnik, R. M. Thorne, and H. Spence (2016), Electron butterfly distribution modulation by magnetosonic waves, *Geophys. Res. Lett.*, *43*, 3051–3059, doi:10.1002/2016GL068161.
- Mauk, B. H., N. J. Fox, S. G. Kanekal, R. L. Kessel, D. G. Sibeck, and A. Ukhorskiy (2013), Science objectives and rationale for the radiation belt storm probes mission, *Space Sci. Rev.*, *179*(1–4), 3–27, doi:10.1007/s11214-012-9908-y.
- Meredith, N. P., A. D. Johnstone, S. Szita, R. B. Horne, and R. R. Anderson (1999), “Pancake” electron distributions in the outer radiation belts, *J. Geophys. Res.*, *104*(A6), 12,431–12,444, doi:10.1029/1998JA000083.
- Mitchell, D. G., et al. (2013), Radiation Belt Storm Probes Ion Composition Experiment (RBSPICE), *Space Sci. Rev.*, *179*(1–4), 263–308, doi:10.1007/s11214-013-9965-x.
- Ni, B., et al. (2015), Variability of the pitch angle distribution of radiation belt ultrarelativistic electrons during and following intense geomagnetic storms: Van Allen probes observations, *J. Geophys. Res. Space Physics*, *120*, 4863–4876, doi:10.1002/2015JA021065.
- Ni, B., Z. Zou, X. Li, J. Bortnik, L. Xie, and X. Gu (2016), Occurrence characteristics of outer zone relativistic electron butterfly distribution: A survey of Van Allen Probes REPT measurements, *Geophys. Res. Lett.*, *43*, 5644–5652, doi:10.1002/2016GL069350.
- Reeves, G. D. (2003), IMAGE, POLAR, and geosynchronous observations of substorm and ring current ion injection, in *Disturbances in Geospace: The Storm-Substorm Relationship*, vol. 142, edited by A. S. Sharma, Y. Kamide, and G. S. Lakhina, 91 pp., AGU, Washington, D. C., doi:10.1029/142GM09.
- Reeves, G. D., et al. (2013), Electron acceleration in the heart of the Van Allen radiation belts, *Science*, *341*(6149), 991–994, doi:10.1126/science.1237743.
- Roederer, J. G. (1967), On the adiabatic motion of energetic particles in a model magnetosphere, *J. Geophys. Res.*, *72*(3), 981–992, doi:10.1029/JZ072i003p00981.
- Selesnick, R. S., and J. B. Blake (2002), Relativistic electron drift shell splitting, *J. Geophys. Res.*, *107*(A9), 1265, doi:10.1029/2001JA009179.
- Sibeck, D. G., R. W. McEntire, A. T. Y. Lui, R. E. Lopez, and S. M. Krimigis (1987), Magnetic field drift shell splitting: Cause of unusual dayside particle pitch angle distributions during storms and substorms, *J. Geophys. Res.*, *92*(A12), 13,485–13,497, doi:10.1029/JA092ia12p13485.
- Su, Z., F. Xiao, H. Zheng, and S. Wang (2010), Combined radial diffusion and adiabatic transport of radiation belt electrons with arbitrary pitch angles, *J. Geophys. Res.*, *115*, A10249, doi:10.1029/2010JA015903.
- Summers, D., B. Ni, and N. P. Meredith (2007), Timescales for radiation belt electron acceleration and loss due to resonant wave-particle interactions: 2. Evaluation for VLF chorus, ELF hiss, and electromagnetic ion cyclotron waves, *J. Geophys. Res.*, *112*, A04207, doi:10.1029/2006JA011993.
- Thorne, R. M., et al. (2013), Rapid local acceleration of relativistic radiation-belt electrons by magnetospheric chorus, *Nature*, *504*(7480), 411–414, doi:10.1038/nature12889.
- Wang, B., Z. Su, Y. Zhang, S. Shi, and G. Wang (2016), Nonlinear Landau resonant scattering of near equatorially mirroring radiation belt electrons by oblique EMIC waves, *Geophys. Res. Lett.*, *43*, 3628–3636, doi:10.1002/2016GL068467.
- West, H. I., R. M. Buck, and J. R. Walton (1973), Electron pitch angle distributions throughout the magnetosphere as observed on OGO 5, *J. Geophys. Res.*, *78*(7), 1064–1081, doi:10.1029/JA078i007p01064.
- Wilken, B., D. N. Baker, P. R. Higbie, T. A. Fritz, W. P. Olson, and K. A. Pfizter (1986), Magnetospheric configuration and energetic particle effects associated with a SSC: A case study of the CDAW 6 event on March 22, 1979, *J. Geophys. Res.*, *91*(A2), 1459–1473, doi:10.1029/JA091ia02p01459.
- Wygant, J. R., et al. (2013), The electric field and waves instruments on the radiation belt storm probes mission, *Space Sci. Rev.*, *179*, 183–220, doi:10.1007/s11214-013-0013-7.
- Xiao, F., C. Yang, Z. Su, Q. Zhou, Z. He, Y. He, D. N. Baker, H. E. Spence, H. O. Funsten, and J. B. Blake (2015), Wave-driven butterfly distribution of Van Allen belt relativistic electrons, *Nat. Commun.*, *6*, 8590, doi:10.1038/ncomms9590.
- Xiong, Y., L. Xie, Z. Pu, S. Fu, L. Chen, B. Ni, W. Li, J. Li, R. Guo, and G. K. Parks (2015), Responses of relativistic electron fluxes in the outer radiation belt to geomagnetic storms, *J. Geophys. Res. Space Physics*, *120*, 9513–9523, doi:10.1002/2015JA021440.
- Zhao, H., X. Li, J. B. Blake, J. F. Fennell, S. G. Claudepierre, D. N. Baker, A. N. Jaynes, and D. M. Malaspina (2014a), Characteristics of pitch angle distributions of hundreds of keV electrons in the slot region and inner radiation belt, *J. Geophys. Res. Space Physics*, *119*, 9543–9557, doi:10.1002/2014JA020386.
- Zhao, H., X. Li, J. B. Blake, J. F. Fennell, S. G. Claudepierre, D. N. Baker, A. N. Jaynes, D. M. Malaspina, and S. G. Kanekal (2014b), Peculiar pitch angle distribution of relativistic electrons in the inner radiation belt and slot region, *Geophys. Res. Lett.*, *41*, 2250–2257, doi:10.1002/2014GL059725.